# Supporting Information for "Morphodynamics of barchan-barchan interactions investigated at the grain scale"

W. R. Assis[1], E. M. Franklin[1]

[1]School of Mechanical Engineering, UNICAMP - University of Campinas,

Rua Mendeleyev, 200, Campinas, SP, Brazil

## Contents of this file

1. Figures S1 to S12

2. Tables S1 and S2

## Additional Supporting Information (Files uploaded separately)

1. Captions for Movies S1 to S22

## Introduction

This supporting information presents microscopy images of the used grains, additional graphics, lists of the tested conditions, and movies showing examples of grains' displacements for each interaction pattern. We note that the images that were processed to plot the figures shown in the paper are available on Mendeley Data (http://dx.doi.org/10.17632/f9p59sxm4f).

―――――

February 13, 2021, 12:01pm

**Movie S1. Chasing_Aligned_t1.gif** Movie showing a sequence of 10 images of the chasing pattern in aligned configuration during a first stage of interaction. It is possible to follow the moving grains in the movie.

**Movie S2. Chasing_Aligned_t2.gif** Movie showing a sequence of 10 images of the chasing pattern in aligned configuration during a second stage of interaction. It is possible to follow the moving grains in the movie.

**Movie S3. Chasing_OffCentered_t1.gif** Movie showing a sequence of 10 images of the chasing pattern in off-centered configuration during a first stage of interaction. It is possible to follow the moving grains in the movie.

**Movie S4. Chasing_OffCentered_t2.gif** Movie showing a sequence of 10 images of the chasing pattern in off-centered configuration during a second stage of interaction. It is possible to follow the moving grains in the movie.

**Movie S5. Merging_Aligned_t1.gif** Movie showing a sequence of 10 images of the merging pattern in aligned configuration during a first stage of interaction. It is possible to follow the moving grains in the movie.

**Movie S6. Merging_Aligned_t2.gif** Movie showing a sequence of 10 images of the merging pattern in aligned configuration during a second stage of interaction. It is possible to follow the moving grains in the movie.

**Movie S7. Merging_OffCentered_t1.gif** Movie showing a sequence of 10 images of the merging pattern in off-centered configuration during a first stage of interaction. It is possible to follow the moving grains in the movie.

**Movie S8. Merging_OffCentered_t2.gif** Movie showing a sequence of 10 images of the merging pattern in off-centered configuration during a second stage of interaction. It is possible to follow the moving grains in the movie.

**Movie S9. Exchange_Aligned_t1.gif** Movie showing a sequence of 10 images of the exchange pattern in aligned configuration during a first stage of interaction. It is possible to follow the moving grains in the movie.

**Movie S10. Exchange_Aligned_t2.gif** Movie showing a sequence of 10 images of the exchange pattern in aligned configuration during a second stage of interaction. It is possible to follow the moving grains in the movie.

**Movie S11. Exchange_OffCentered_t1.gif** Movie showing a sequence of 10 images of the exchange pattern in off-centered configuration during a first stage of interaction. It is possible to follow the moving grains in the movie.

**Movie S12. Exchange_OffCentered_t2.gif** Movie showing a sequence of 10 images of the exchange pattern in off-centered configuration during a second stage of interaction. It is possible to follow the moving grains in the movie.

**Movie S13. FragChasing_Aligned_t1.gif** Movie showing a sequence of 10 images of the fragmentation-chasing pattern in aligned configuration during a first stage of interaction. It is possible to follow the moving grains in the movie.

**Movie S14. FragChasing_Aligned_t2.gif** Movie showing a sequence of 10 images of the fragmentation-chasing pattern in aligned configuration during a second stage of interaction. It is possible to follow the moving grains in the movie.

**Movie S15. FragChasing_Aligned_t3.gif** Movie showing a sequence of 10 images of the fragmentation-chasing pattern in aligned configuration during a third stage of interaction. It is possible to follow the moving grains in the movie.

**Movie S16. FragChasing_OffCentered_t1.gif** Movie showing a sequence of 10 images of the fragmentation-chasing pattern in off-centered configuration during a first stage of interaction. It is possible to follow the moving grains in the movie.

**Movie S17. FragChasing_OffCentered_t2.gif** Movie showing a sequence of 10 images of the fragmentation-chasing pattern in off-centered configuration during a second stage of interaction. It is possible to follow the moving grains in the movie.

**Movie S18. FragChasing_OffCentered_t3.gif** Movie showing a sequence of 10 images of the fragmentation-chasing pattern in off-centered configuration during a third stage of interaction. It is possible to follow the moving grains in the movie.

**Movie S19. FragExchange_Aligned_t1.gif** Movie showing a sequence of 10 images of the fragmentation-exchange pattern in aligned configuration during a first stage of interaction. It is possible to follow the moving grains in the movie.

**Movie S20. FragExchange_Aligned_t2.gif** Movie showing a sequence of 10 images of the fragmentation-exchange pattern in aligned configuration during a second stage of interaction. It is possible to follow the moving grains in the movie.

**Movie S21. FragExchange_OffCentered_t1.gif** Movie showing a sequence of 10 images of the fragmentation-exchange pattern in off-centered configuration during a first stage of interaction. It is possible to follow the moving grains in the movie.

**Movie S22. FragExchange_OffCentered_t2.gif** Movie showing a sequence of 10 im-
ages of the fragmentation-exchange pattern in off-centered configuration during a second
stage of interaction. It is possible to follow the moving grains in the movie.
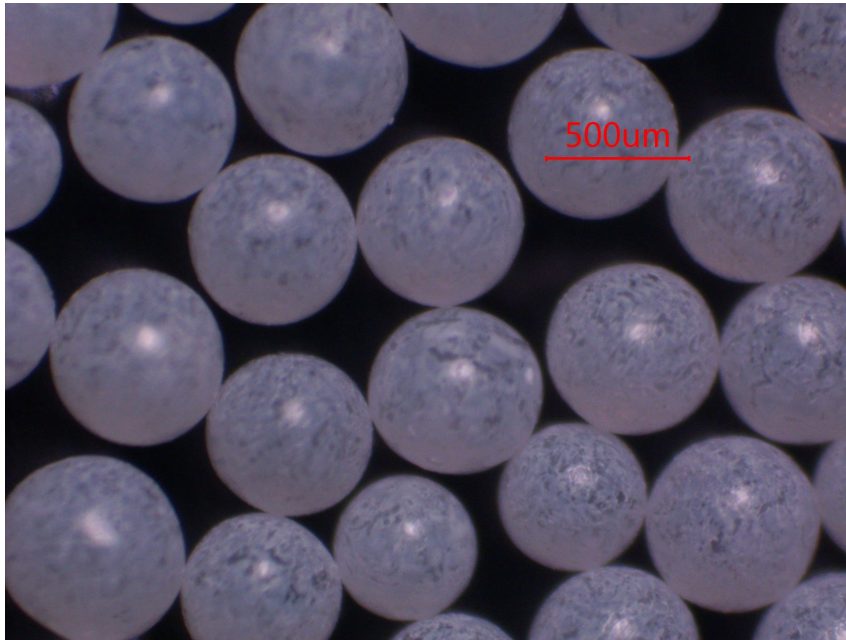


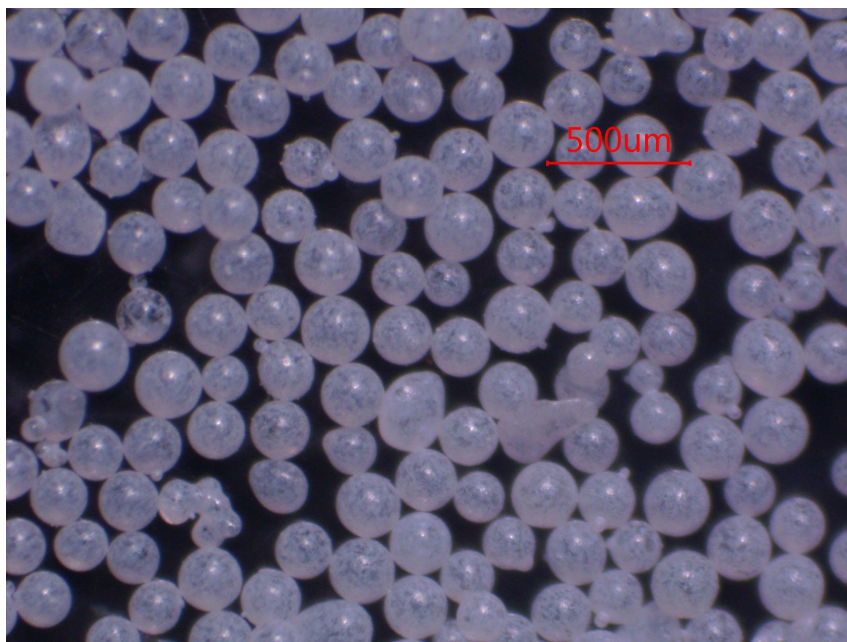**Figure S1.**  Microscopy image for the 0.40 mm $\leq d \leq$ 0.60 mm round glass beads of white
color.
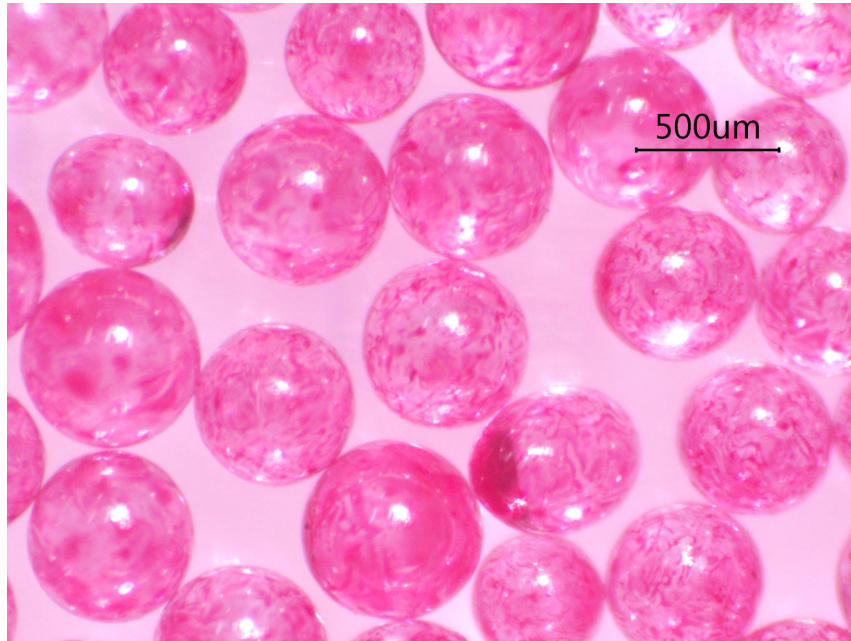
**Figure S2.** Microscopy image for the 0.40 mm $\leq d \leq$ 0.60 mm round glass beads of red color.
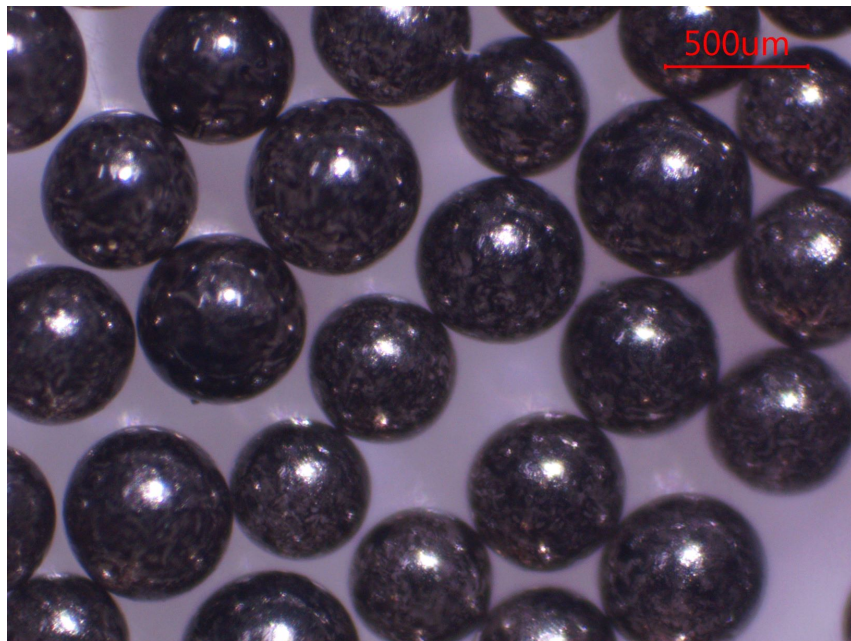


**Figure S3.** Microscopy image for the 0.40 mm $\leq d \leq$ 0.60 mm round glass beads of black color.

February 13, 2021, 12:01pm

**Figure S4.**    Microscopy image for the 0.15 mm $\leq d \leq$ 0.25 mm round glass beads of white color.



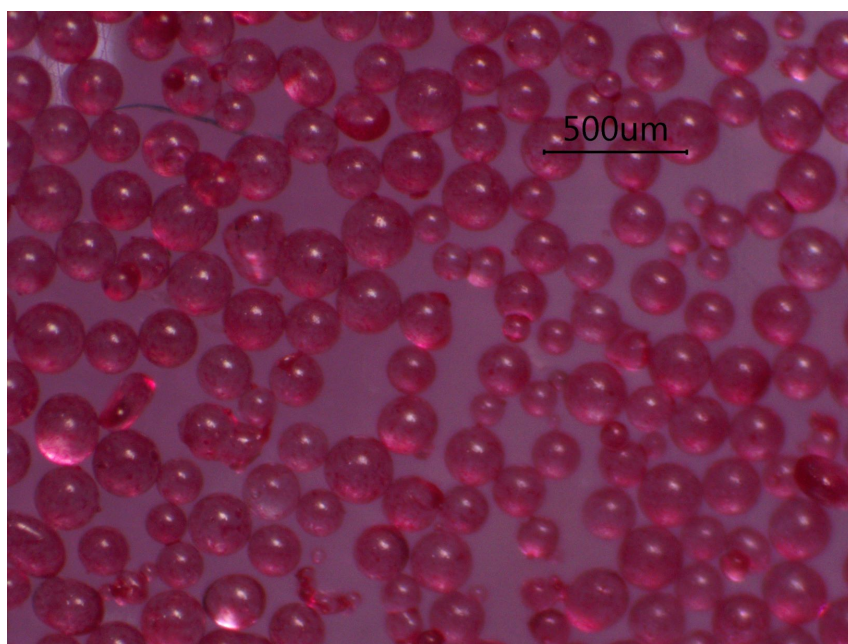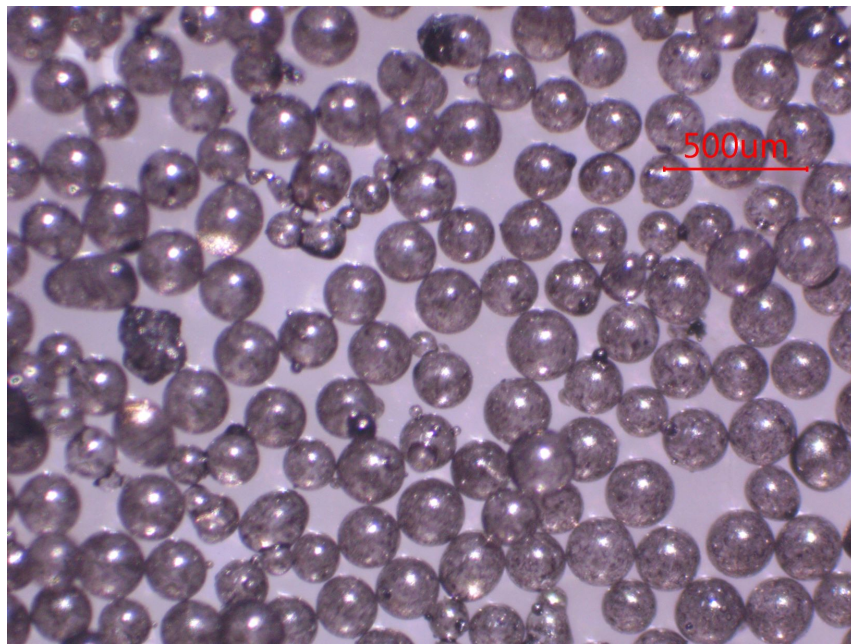**Figure S5.**    Microscopy image for the 0.15 mm $\leq d \leq$ 0.25 mm round glass beads of red color.

:



**Figure S6.** Microscopy image for the 0.15 mm $\leq d \leq$ 0.25 mm round glass beads of black color.
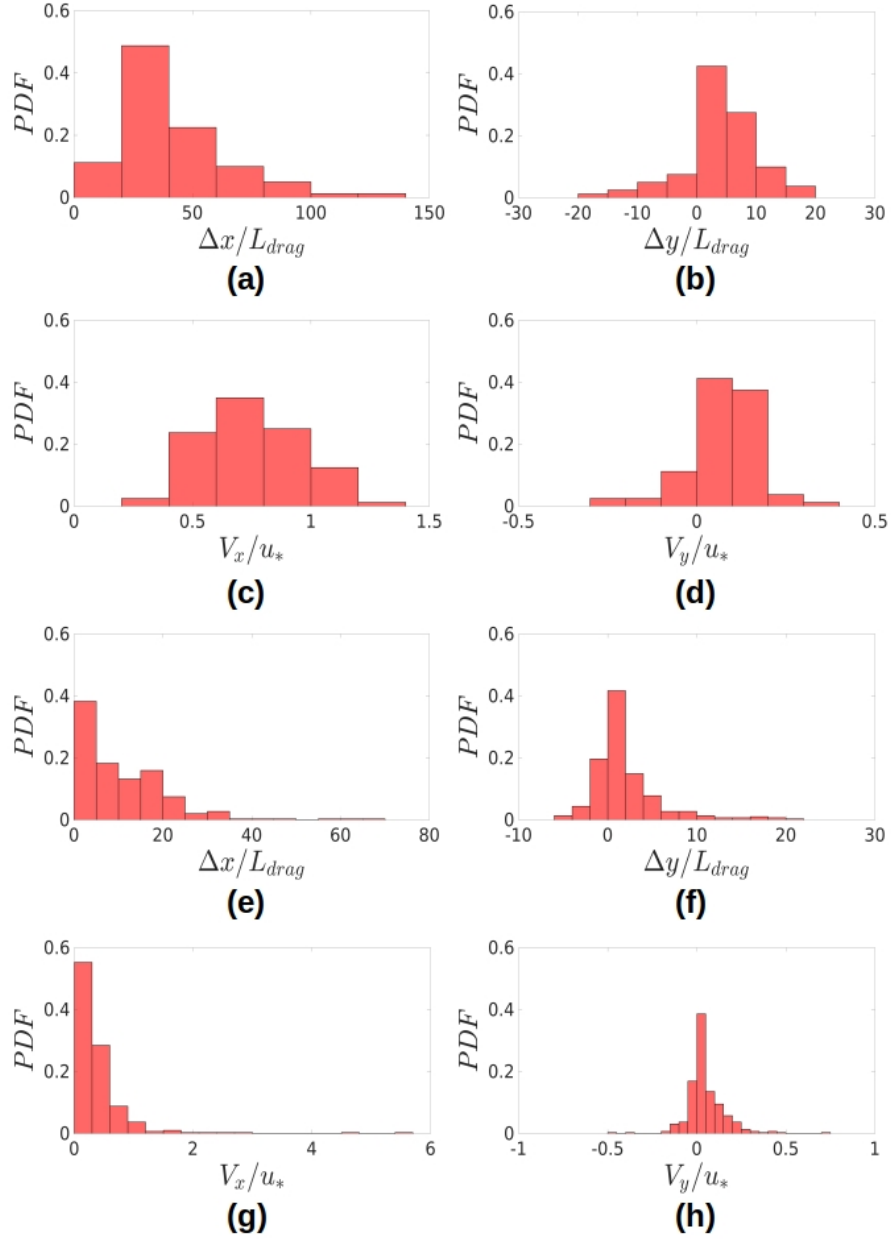
**Figure S7.** Probability distribution functions (PDFs), for grains exchanged between barchans, of total distances traveled by grains, $\Delta x$ and $\Delta y$, and time-averaged velocities, $V_x$ and $V_y$. Figures (a) to (d) correspond to the chasing pattern (red trajectories in Figure 2d of the paper) and Figures (e) to (h) to the merging pattern (red trajectories in Figure 3b of the paper).
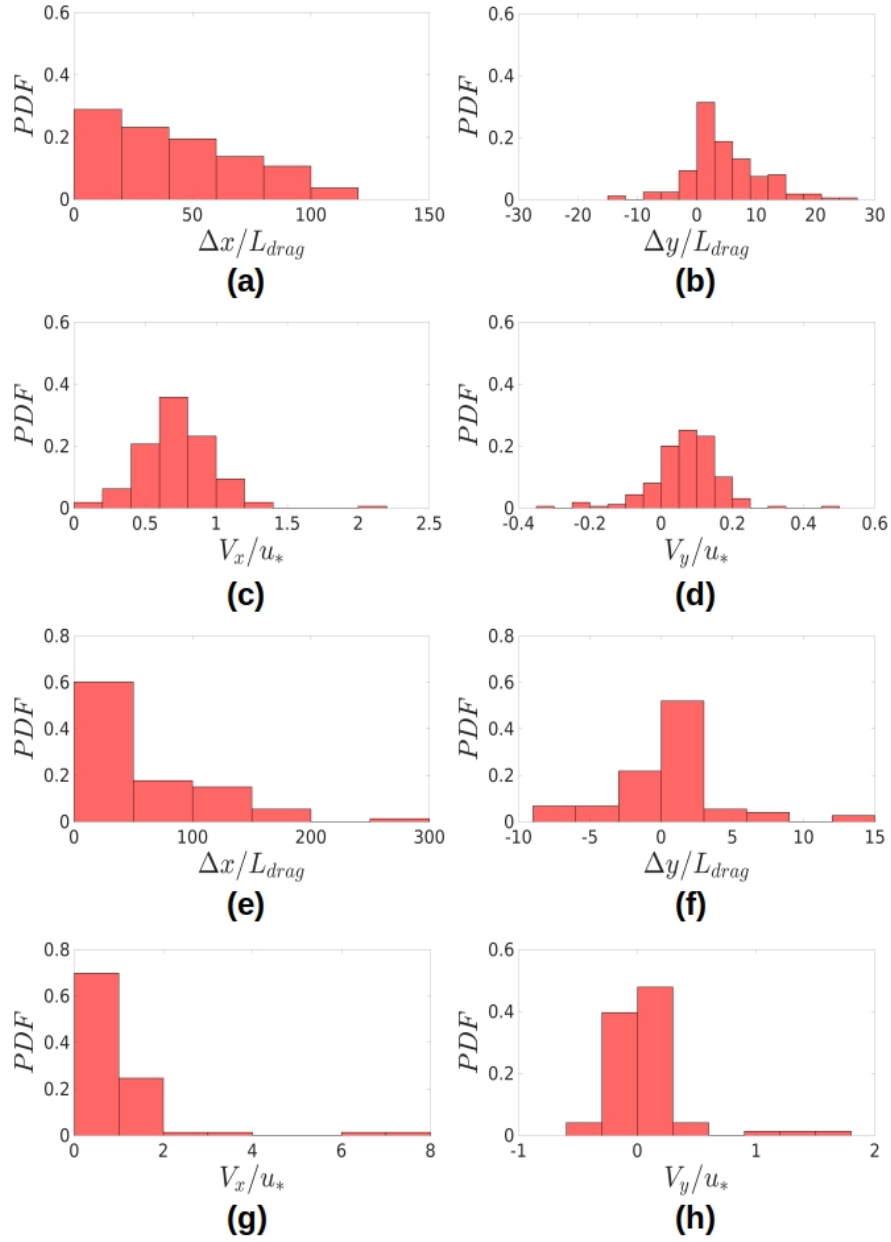
**Figure S8.** Probability distribution functions (PDFs), for grains exchanged between barchans, of total distances traveled by grains, $\Delta x$ and $\Delta y$, and time-averaged velocities, $V_x$ and $V_y$. All figures concern the fragmentation-chasing pattern, Figures (a) to (d) corresponding to the red trajectories in Figure 5a of the paper and Figures (e) to (h) to the red trajectories in Figure 5f of the paper.
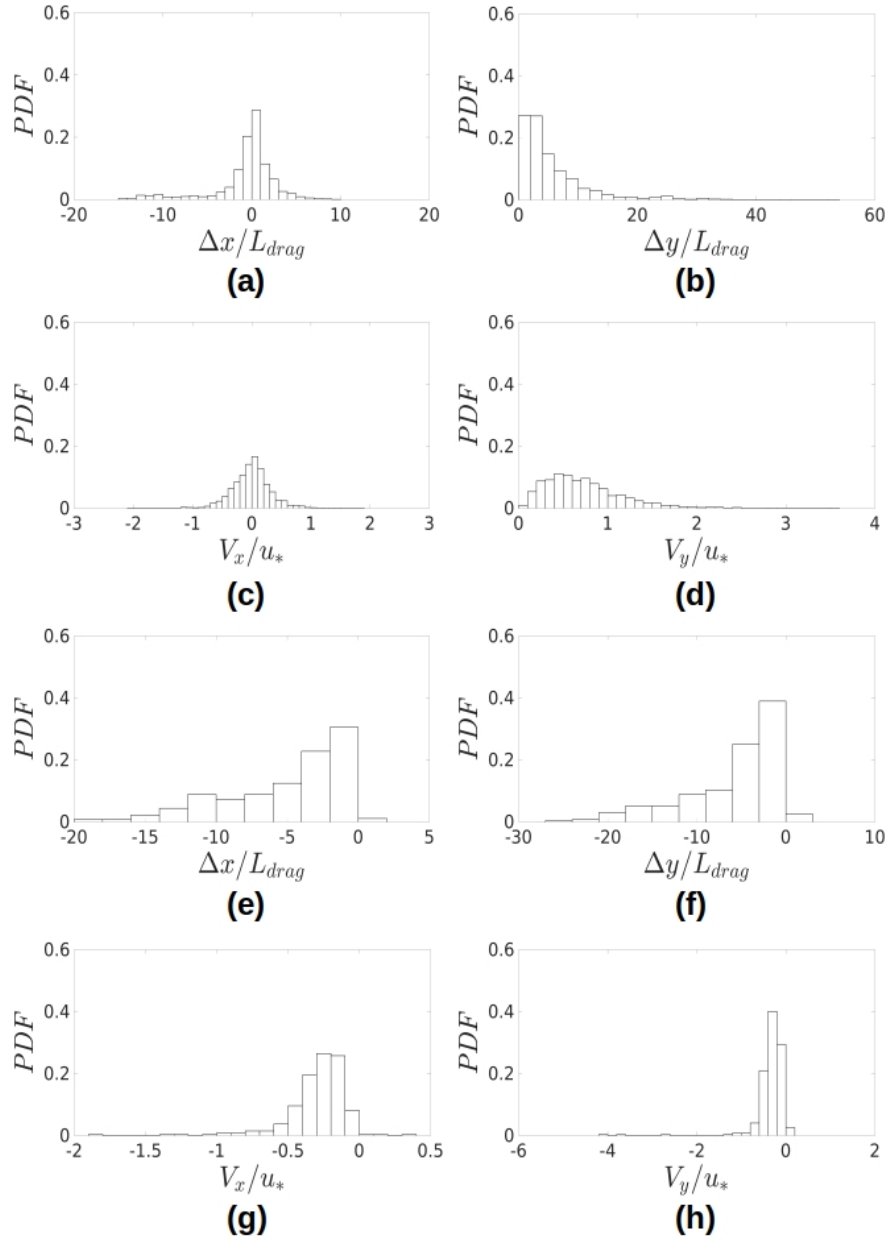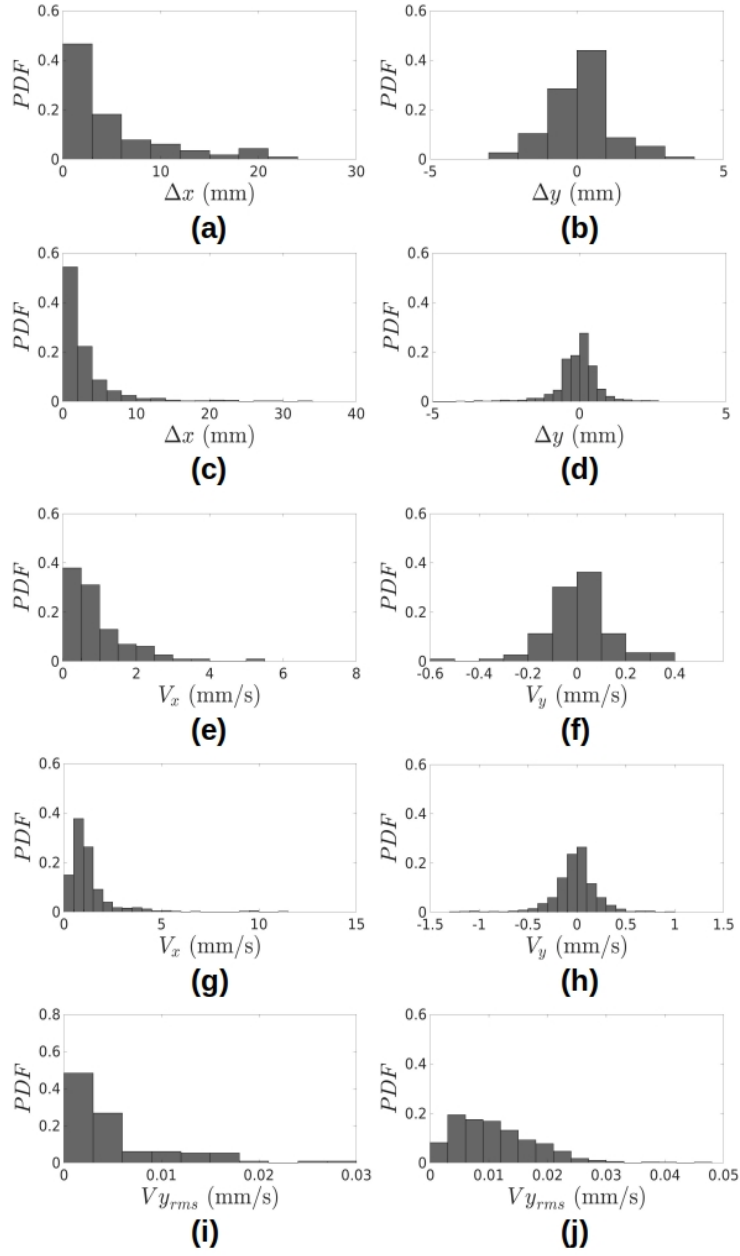
**Figure S9.** Probability distribution functions (PDFs), for grains exchanged between barchans, of total distances traveled by grains, $\Delta x$ and $\Delta y$, and time-averaged velocities, $V_x$ and $V_y$. Figures (a) to (d) correspond to the fragmentation-exchange pattern (white trajectories in Figure 6c of the paper) and Figures (e) to (h) to the exchange pattern (white trajectories in Figure 4d of the paper).

:



**Figure S10.** Probability distribution functions (PDFs), for grains from the impact barchan spreading over the target one, of total distances traveled by grains, $\Delta x$ and $\Delta y$, time-averaged velocities, $V_x$ and $V_y$, and RMS averages of the transverse velocity of each grain $Vy_{rms}$, in dimensional form. Figures (a),(b),(e),(f) and (i) correspond to the merging pattern and Figures (c),(d),(g),(h) e (j) to the exchange pattern.

| | Chasing | | | |
|---|---|---|---|---|
| Figure paper | Going over downstream barchan | Going around downstream barchan | Directly entrained downstream | Flux difference |
| 2b | 24% | 7% | 69% | 18% |
| 2d | 28% | 44% | 28% | 33% |
| | Merging | | | |
| Figure paper | Going over downstream barchan + going around downstream barchan | | | |
| 3a | 92% | | | |
| 3c | 1% | | | |
| | Exchange | | | |
| Figure paper | Migrating from the new ejected barchan (baby barchan) toward the upstream bedform | | | |
| 4b | 22% | | | |
| | Frag-Chasing | | | |
| Figure paper | Flux difference | | | |
| 5a | 64% | | | |
| 5d | 19% | | | |
| | Frag-Exchange | | | |
| Figure paper | Grains entrained from the downstream bedform toward the impact barchan | | | |
| 6a | 46% | | | |
| 6b | 42% | | | |
| 6c | 70% | | | |
| 6d | 5% | | | |

**Figure S11.** Percentages of grains exchanged between dunes for some cases presented in the paper. The column *Figure paper* lists the corresponding figure numbers in the paper.

| Pattern | Chasing | | | Merging | | | Exchange | |
|---|---|---|---|---|---|---|---|---|
| Figure (paper) | 2a | 2b | 2c | 3a | 3b | 3d | 4b | 4d |
| mean $V_x$ / $u_*$ | 1.31 | 1.13 | 0.75 | 0.71 | 0.41 | 0.62 | 0.55 | -0.29 |
| Standard deviation $V_x/u_*$ | 0.54 | 0.34 | 0.22 | 0.37 | 0.54 | 0.46 | 0.31 | 0.22 |
| mean $V_y/u_*$ | -0.01 | 0.23 | 0.07 | 0.06 | 0.05 | 0.04 | 0.37 | -0.34 |
| Standard deviation $V_y/u_*$ | 0.16 | 0.10 | 0.10 | 0.14 | 0.11 | 0.10 | 1.13 | 0.40 |
| Mean $\Delta x/L_{drag}$ | 55.18 | 34.45 | 40.74 | 33.39 | 10.80 | 12.56 | 9.11 | -5.06 |
| Standard deviation $\Delta x/L_{drag}$ | 28.32 | 14.27 | 23.55 | 18.16 | 10.30 | 12.70 | 5.35 | 4.27 |
| Mean $\Delta y/L_{drag}$ | -0.11 | 6.90 | 3.75 | 2.44 | 1.96 | 1.25 | 8.01 | -5.76 |
| Standard deviation $\Delta y/L_{drag}$ | 5.96 | 3.70 | 6.35 | 6.65 | 3.92 | 2.37 | 17.83 | 5.35 |
| Pattern | Frag-chasing | | | | | Frag-exchange | | |
| Figure (paper) | 5a | 5b | 5c | 5e | 5f | 6a | 6c | |
| mean $V_x$ / $u_*$ | 0.73 | 1.01 | 1.01 | 1.21 | 1.01 | -0.10 | 0.00 | |
| Standard deviation $V_x/u_*$ | 0.26 | 0.45 | 0.39 | 0.30 | 1.12 | 0.06 | 0.33 | |
| mean $V_y/u_*$ | 0.07 | -0.01 | -0.08 | 0.03 | 0.07 | -0.14 | 0.72 | |
| Standard deviation $V_y/u_*$ | 0.10 | 0.21 | 0.19 | 0.10 | 0.31 | 0.18 | 0.43 | |
| Mean $\Delta x/L_{drag}$ | 41.79 | 47.30 | 35.31 | 130.43 | 47.85 | -7.16 | -0.66 | |
| Standard deviation $\Delta x/L_{drag}$ | 30.41 | 30.69 | 28.92 | 54.05 | 59.51 | 3.51 | 3.51 | |
| Mean $\Delta y/L_{drag}$ | 4.58 | -2.71 | -2.81 | 2.66 | 0.13 | -6.26 | 5.50 | |
| Standard deviation $\Delta y/L_{drag}$ | 6.18 | 10.62 | 7.65 | 8.36 | 3.75 | 11.36 | 6.02 | |

**Figure S12.** Mean values and standard deviations of $\Delta x$, $\Delta y$, $V_x$ and $V_y$ for the trajectories indicated in the line *Figure (paper)*, which lists the corresponding figure numbers in the paper. The colors of the cells are the same as those of trajectories in the corresponding figure.

:

**Table S1.** List of the tested conditions in the aligned configuration. $\sigma$ is the offset parameter, $m_i$ and $m_t$ are the masses of the impacting (upstream) and target (downstream) dunes, respectively, $N_i$ and $N_t$ are the numbers of grains of the impacting and target dunes, respectively, $\xi_N$ is the dimensionless particle number, $\rho_s$ and $d$ are the density and mean diameter of grains, respectively, $u_*$ is the shear velocity, $Re_*$ is the particle Reynolds number, $\theta$ is the Shields number, and *Pattern* corresponds to the collision pattern. For definitions of $\sigma$ and $\xi_N$, please refer to Assis and Franklin, Geophys. Res. Lett., 47, e2020GL089464, 2020, https://doi.org/10.1029/2020GL089464.

| $\sigma$ | $m_i$ | $m_t$ | $N_i$ | $N_t$ | $\xi_N$ | $\rho_s$ | $d$ | $u_*$ | $Re_*$ | $\theta$ | Pattern |
|---|---|---|---|---|---|---|---|---|---|---|---|
| $\cdots$ | g | g | $\cdots$ | $\cdots$ | $\cdots$ | kg/m$^3$ | mm | m/s | $\cdots$ | $\cdots$ | $\cdots$ |
| 0.06 | 10.0 | 10.0 | 61115 | 61115 | 0.00 | 2500 | 0.5 | 0.0159 | 3 | 0.086 | Chasing |
| 0.07 | 1.0 | 8.0 | 6112 | 48892 | 0.78 | 2500 | 0.5 | 0.0141 | 7 | 0.027 | Merging |
| 0.04 | 0.3 | 14.0 | 28648 | 1336902 | 0.96 | 2500 | 0.2 | 0.0159 | 3 | 0.086 | Exchange |
| 0.07 | 2.0 | 8.0 | 190986 | 763944 | 0.60 | 2500 | 0.2 | 0.0159 | 3 | 0.086 | Frag.-chasing |
| 0.03 | 1.0 | 8.0 | 95493 | 763944 | 0.78 | 2500 | 0.2 | 0.0141 | 3 | 0.068 | Frag.-exchange |

**Table S2.** List of the tested conditions in the off-centered configuration. $\sigma$ is the offset parameter, $m_i$ and $m_t$ are the masses of the impacting (upstream) and target (downstream) dunes, respectively, $N_i$ and $N_t$ are the numbers of grains of the impacting and target dunes, respectively, $\xi_N$ is the dimensionless particle number, $\rho_s$ and $d$ are the density and mean diameter of grains, respectively, $u_*$ is the shear velocity, $Re_*$ is the particle Reynolds number, $\theta$ is the Shields number, and *Pattern* corresponds to the collision pattern. For definitions of $\sigma$ and $\xi_N$, please refer to Assis and Franklin, Geophys. Res. Lett., 47, e2020GL089464, 2020, https://doi.org/10.1029/2020GL089464.

| $\sigma$ | $m_i$ | $m_t$ | $N_i$ | $N_t$ | $\xi_N$ | $\rho_s$ | $d$ | $u_*$ | $Re_*$ | $\theta$ | Pattern |
|---|---|---|---|---|---|---|---|---|---|---|---|
| $\cdots$ | g | g | $\cdots$ | $\cdots$ | $\cdots$ | kg/m$^3$ | mm | m/s | $\cdots$ | $\cdots$ | $\cdots$ |
| 0.60 | 10.0 | 10.0 | 61115 | 61115 | 0.00 | 2500 | 0.5 | 0.0141 | 7 | 0.027 | Chasing |
| 0.53 | 1.0 | 8.0 | 6112 | 48892 | 0.78 | 2500 | 0.5 | 0.0141 | 7 | 0.027 | Merging |
| 0.36 | 0.5 | 6.0 | 47746 | 572958 | 0.85 | 2500 | 0.2 | 0.0159 | 3 | 0.086 | Exchange |
| 0.29 | 6.0 | 8.0 | 572958 | 763944 | 0.14 | 2500 | 0.2 | 0.0159 | 3 | 0.086 | Frag.-chasing |
| 0.33 | 2.0 | 8.0 | 190986 | 763944 | 0.60 | 2500 | 0.2 | 0.0159 | 3 | 0.086 | Frag.-exchange |